Int J Mech Mater Des (2016) 12:495–507
DOI 10.1007/s10999-016-9350-5

Discrete element simulation of dynamic behaviour of partially saturated sand

E. A. Flores-Johnson · S. Wang · F. Maggi · A. El Zein · Y. Gan · G. D. Nguyen · Luming Shen

Received: 2 November 2015 / Accepted: 9 August 2016 / Published online: 13 August 2016

Abstract The discrete element method (DEM) together with the finite element method (FEM) in LS-DYNA was employed to investigate the dynamic behaviour of sand under impact loading. In this approach, the partially saturated sand was modelled in DEM with capillary forces being taken into account through an implicit capillary contact model, while other solids were simulated using FEM. A slump test was first performed with dry sand to calibrate the contact parameters in DEM. Low velocity impact tests were then conducted to investigate the effect of water saturation on the shape and height of sand piles after impact, and to validate the simulations. It was found in the experiments that an increasing water saturation (in the range between 10 and 30 %) affected the height of sand pile for a given drop height due to an increasing cohesion between particles. The simulations captured the experimental ejecta patterns and sand pile height. Finally, a low confinement split Hopkinson pressure bar test from earlier literature was modelled; the DEM–FEM simulations could reproduce the trends of experimentally observed stress–strain curves of partially saturated sand under high strain rate loading, indicating that it was feasible to model dynamic behaviour of dry and wet sand with low saturation (<20 %) in LS-DYNA; however, a number of questions remain open about the effect of grain shape, grain crushing and viscosity.

Keywords Partially saturated sand · Impact · Capillary force · Discrete element method · DEM–FEM simulation · LS-DYNA

E. A. Flores-Johnson · S. Wang · F. Maggi · A. El Zein · Y. Gan · L. Shen (✉)
School of Civil Engineering, The University of Sydney, Sydney, NSW 2006, Australia
e-mail: Luming.Shen@sydney.edu.au

E. A. Flores-Johnson
e-mail: Emmanuel.Flores-Johnson@sydney.edu.au

S. Wang
e-mail: Shengzhe.Wang@sydney.edu.au

F. Maggi
e-mail: Federico.Maggi@sydney.edu.au

A. El Zein
e-mail: Abbas.El-Zein@sydney.edu.au

Y. Gan
e-mail: Yixiang.Gan@sydney.edu.au

G. D. Nguyen
School of Civil, Environmental and Mining Engineering, The University of Adelaide, Adelaide, SA 5005, Australia
e-mail: g.nguyen@adelaide.edu.au

1 Introduction

The behaviour of partially saturated soil subjected to dynamic loading conditions such as blast, impact or seismic loading has become an interesting and challenging topic for engineering applications in geotechnical and civil engineering (Shahbodagh-Khan et al.

2015). It is well known that the water saturation (or water content) in soil affects its physical properties and mechanical performance, particularly when loading is dynamic (Omidvar et al. 2012; Martin et al. 2009). These effects occur mainly due to a complex interaction between solid grains, pore water and pore air (Martin et al. 2009; Saleh and Edwards 2015). While significant advances have been achieved in our understanding of single-phase (dry) and two-phase (water-saturated) soils under dynamic loading (Shahbodagh-Khan et al. 2015), and partially saturated soils under quasi-static loading (Mitarai and Nori 2006), understanding of dynamic behaviour of partially saturated soils is still at early stages. In quasi-static loading conditions, it is known that saturation affects the stress–strain response of sand because of capillary forces (Mitarai and Nori 2006); however, for high strain-rate loading conditions, the response may be dominated by water, air, solid particles, or the interaction of these three phases. Experimental observations of high strain-rate behaviour of a partially saturated sand using the split Hopkinson pressure bar (SHPB) (Martin et al. 2009; Veyera 1994) have shown that the stiffness of a confined specimen depends on the water saturation. For saturations smaller than 20 %, the stiffness was found to degrade as water content increases, starting from dry sand. Martin et al. (Martin et al. 2009) explained that this could be attributed to water lubrication between grains. For saturations greater than 20 %, stiffness larger than that of the dry sand has been observed (Veyera 1994). At large strains and strain rates, this response is accompanied by a lock-up behaviour mainly dominated by pore water (Omidvar et al. 2012). However, experimental results from Horn and Deere (Horn and Deere 1962) of direct shear tests performed on Ottawa sand showed that variations in the sand surface moisture does not have a significant effect on the shear resistance aside from some possible capillary forces effect (Omidvar et al. 2012). The abovementioned non-monotonic response of stiffness to increasing water content necessitates the need to better understand the high strain-rate response of partially saturated soil.

Recent studies on low- and intermediate-velocity impact of sand have also demonstrated that the dynamic response of partially saturated sand depends on the saturation. Takita and Sumita (Takita and Sumita 2013) showed that the shape and diameter of a crater caused by a spherical rigid impactor with a given impact velocity and diameter largely depends on the water saturation, which was varied from 0 to 65 %. Park et al. (Park et al. 2013) found substantial differences in impact of a sand slug on a rigid surface between dry and wet sand for an impact velocity around 100 m/s. They observed that dry sand slugs lengthened faster than the wet sand slugs during travel from the launch apparatus before hitting the target. They also observed that wet sand slugs exhibited a mushrooming head shape and concluded that the relation between the ejecta characteristics and the properties of the densified sand were unclear and hence further numerical modelling was needed to understand these relationships (Park et al. 2013). A clear understanding of the mechanical response of partially saturated soils to extreme events such as blast, impact or earthquake loadings, where dynamic loading can occur, is crucial for the design of essential infrastructure, e.g., roads, government buildings or power plants. Prohibiting costs of large-scale experimental testing of partially saturated media under extreme loading makes computational approaches more convenient not only to save resources but also to gain an understanding of the mechanical behaviour at different scales.

Numerical simulations have been used in several studies to predict the mechanical behaviour of soil subjected to dynamics loads (Saleh and Edwards 2015; Kong et al. 2014; Li and Flores-Johnson 2011; Omidvar et al. 2014; Børvik et al. 2011; Borg et al. 2013). These simulations include the use of constitutive models of granular media described as a continuum, and the use of particle methods to model granular media at the mesoscale. Continuum constitutive models at the macroscale can be computationally efficient when compared to mesoscale particle models; however, experimental tests are usually required to calibrate constitutive model parameters. Mesoscale models using particle methods are normally computationally expensive; however, they are increasingly being used as an alternative to experimental tests due to significant advances in computing powers over the last few years (Børvik et al. 2011).

The discrete element method (DEM) is a particle-based numerical method that has been extensively used to study granular and soil media (Alonso-Marroquín and Herrmann 2005; Alonso-Marroquín and Wang 2009; Gan and Kamlah 2010) and the

dynamic flow of particles (Alonso-Marroquín et al. 2013). DEM has been employed to understand the dynamic behaviour of dry sand subjected to ballistic (Dwivedi et al. 2008; Oñate and Rojek 2004) and blast (Børvik et al. 2011) loading. There have also been attempts to model the effects of saturation in granular media using implicit capillary forces (Scholtès et al. 2009) in quasi-static conditions (Grima and Wypych 2011; Gröger et al. 2003). However, a full understanding through DEM modelling of the effect of capillary forces on the dynamic behaviour of partially saturated soils is still limited. Therefore, more grain scale and/or multiscale simulations are still needed to develop analytical models with micro/meso scale features that can be implemented in continuum models (Gan et al. 2013).

In this paper, we employ DEM together with the finite-element method (FEM) in the commercial software LS-DYNA for the modelling of partially saturated sand subjected to impact loading. We focus on the feasibility of using the capillary contact model for DEM grains implemented implicitly in LS-DYNA to model wet sand under impact loading. Experimental testing performed to calibrate and validate DEM–FEM simulations is described in Sect. 2. The numerical methods are described in Sect. 3. Results are then presented and discussed in Sect. 4 followed by conclusions and recommendations for future research.

2 Experimental methods

Experiments with dry sand were carried out to calibrate the friction between particles and between particles and FEM surfaces in the DEM–FEM simulations. A slump test was carried out on a poorly graded dry sand to obtain the angle of repose, which is the maximal angle that a surface of a stationary sand pile makes with the horizontal plane under the effect of the gravitational acceleration (Elperin and Golshtein 1997). Subsequently, low velocity impact tests of a sand column on a hard surface were carried out to explore the effect of various saturations on the impact dynamics and validate the DEM–FEM simulations.

2.1 Sand

Poorly graded river sand (Fig. 1a) was adopted for this work. The sand had a specific gravity of 2.65 and was reconstructed such that most grains were within the range of 0.212–0.5 mm in size. To produce this mix, river sand samples were passed through a series of sieves ranging from 0.212 up to 0.5 mm in caliber. The sand retained on each sieve was subsequently transferred to separate containers and combined into a single mix according to the required mass proportions represented in Fig. 1b. This was accomplished using an electronic scale to ensure that the correct mass of each size range was being incorporated into the final mix. This sand mix was used in the experiments.

2.2 Slump test on a horizontal surface

Slump test has been successfully used to calibrate DEM parameters for numerical simulations of coal (Grima and Wypych 2011). In this study, slump tests were performed using the setup shown in Fig. 2a and dry sand described in previous section. These tests were performed to calibrate DEM parameters in LS-DYNA: rolling friction between DEM particles (parameter *fricr*) and dynamic friction between DEM particles and FEM steel surfaces (parameter *fricd*). In these tests, a tube with inner diameter of 14 mm and height of 8 mm filled with dry sand was placed on a rigid clean steel plate. Next, the tube was lifted at a constant speed and angle of repose and height of the sand bulk were measured. The tests were repeated three times.

2.3 Low velocity impact of sand on hard surface (drop test)

Low velocity impact drop tests were conducted on partially saturated sand. The initial dry density of samples was maintained at 1410 kg/m^3, which corresponds to a void ratio (e) of approximately 0.88, defined as the ratio of the volume of voids (V_v) to the volume of solids (V_s) calculated as follows:

$$e = \frac{V_v}{V_s} = \frac{G_s \gamma_w}{\gamma_d} - 1 \tag{1}$$

where G_s is the material specific gravity, γ_w is the unit weight of water and γ_d is the dry specimen density. The testing apparatus consisted of an elevated clamp securing an aluminum ring (Fig. 2b) with an inner diameter of 14 mm and length of 8 mm designed to contain the sample. Saturation values of 10, 20 and 30 % were considered, enabling the required volume of water in milliliters to be derived as follows:

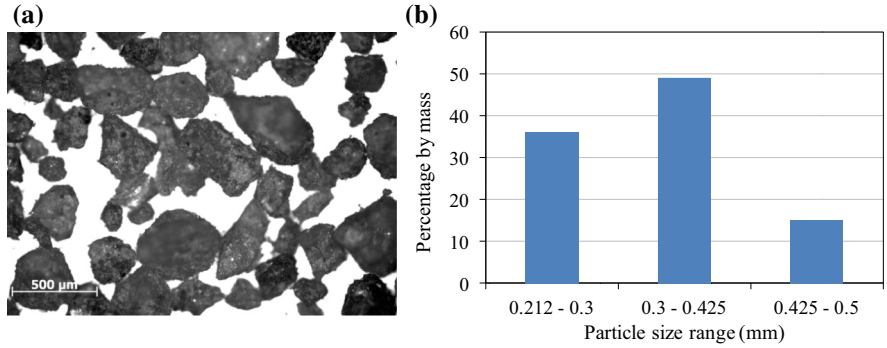

Fig. 1 **a** Microscope image of poorly graded river sand and **b** its particle size distribution

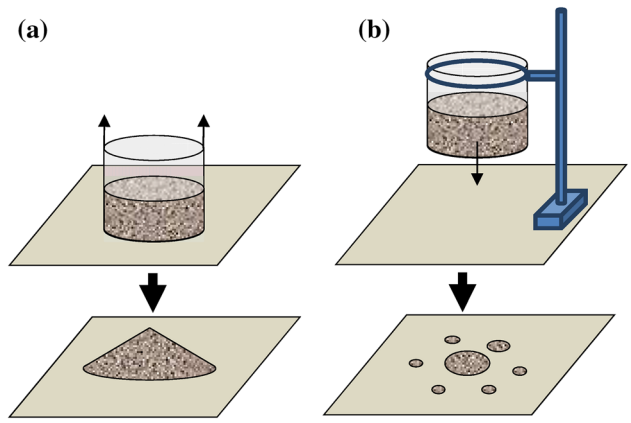

Fig. 2 Schematics of **a** slump tests and **b** drop tests

$$v = m_s\left[\frac{S}{G_s}\left(\frac{G_s\gamma_w}{\gamma_d} - 1\right)\right] = m_s\left(\frac{Se}{G_s}\right) \quad (2)$$

where m_s is the dry specimen mass in grams and S is the saturation. The amount of water to achieve 10, 20 and 30 % saturation corresponded to 0.057, 0.114 and 0.171 ml, respectively. All samples were prepared by first placing 1.74 g of oven-dried river sand in a small plastic container. A micropipette was used to add a quantity of water into the mix necessary to achieve the desired S. The specimen was mechanically shaken to ensure uniform water distribution, and was subsequently transferred into the chamber ring where it was supported by a hatch at the base. The commencement of impact testing involved removing the hatch and gently tapping the side of the chamber to dislodge the specimen. This allowed the partially saturated sample to fall from a height h onto a hard steel surface under the influence of the gravitational acceleration. The specimen chamber was weighed before and after testing which confirmed that any potential water loss during the testing process was less than 5 %. Two drop heights h (from the steel surface to the centre of the specimen) of 25 and 75 cm were considered, which produced estimated impact velocities v_i of 2.2 and 3.8 m/s, respectively. The impact velocity was estimated according to the free fall formula, $v_i = \sqrt{2gh}$, where g is the gravitational acceleration; for low drop heights, the abovementioned formula gives a good estimation of v_i (Flores-Johnson and Li 2011). The resulting splash patterns, for each h and S, were photographed and the height H of the sand piles in the middle section was measured. The tests were repeated three times for each condition.

3 DEM–FEM approach

3.1 Discrete element method in LS-DYNA

The DEM implemented in LS-DYNA is based on the method first developed by Cundall and Strack (Cundall and Strack 1979; Hallquist 2015). In LS-DYNA, granular material is described by rigid spherical particles and the interaction of these spheres captures

the bulk behaviour of the material (Jensen et al. 2014). The translational and rotational motion of each particle are computed for each time step Δt using Newton's laws of particle (Pandey et al. 2007). Interaction between particles is handled by penalty-based contact algorithms (Wriggers and 2006). Figure 3a shows a schematic contact interaction between two particles (Karajan et al. 2014). Normal contact forces are defined as (Karajan et al. 2012),

$$F_n = K_n d_{int} \tag{3}$$

where $d_{int} = r_1 + r_2 - |\boldsymbol{X}_1 - \boldsymbol{X}_2|$ is the interaction distance (Fig. 3a) with $\boldsymbol{X}_i$ denoting the coordinates of the i^{th} particle. The normal spring constant K_n is defined as,

$$K_n = \frac{k_1 r_1 k_2 r_2}{k_1 r_1 + k_2 r_2} NORMK \tag{4}$$

where k_i and r_i are the compression moduli and radii of the ith particle, respectively, and *NORMK* is a user-specified stiffness penalty parameter. The parameter $k_i = E_i/3(1-2v_i)$ is calculated in LS-DYNA from the user-specified particle's Young's modulus E and the Poisson's ratio v (Karajan et al. 2014). *NORMK* can be adjusted so as to produce larger or smaller time steps by changing artificially the stiffness in the DEM critical time step (Karajan et al. 2015),

$$\Delta t_{DEM} = TSSFAC\sqrt{\frac{m}{K_n}} \tag{5}$$

where *TSSFAC* is scale factor for computed time step and m is the mass of the DEM particle. The default value of *NORMK* (0.01) in LS-DYNA (Karajan et al. 2012) was used in our simulations. The tangential spring constant is given by (Karajan et al. 2014),

$$K_t = K_n SHEARK \tag{6}$$

where the default value of the stiffness parameter *SHEARK* (used in our simulations) is 2/7 (Karajan et al. 2014). The normal damping force is defined as (Karajan et al. 2014),

$$F_{ndamp} = D_n \dot{d}_{int} \tag{7}$$

where the damping constant D_n is given by,

$$D_n = 2NDAMP\sqrt{\frac{m_1 m_2}{m_1 + m_2} K_n} \tag{8}$$

NDAMP is the normal damping parameter ($0 \leq NDAMP \leq 1$). The tangential damping force is defined in a similar way as Eq. (8) with *TDAMP* and K_t being used instead of *NDAMP* and K_n, respectively. Frictional force F_{fr} is based on Coulomb's law of friction (Karajan et al. 2014),

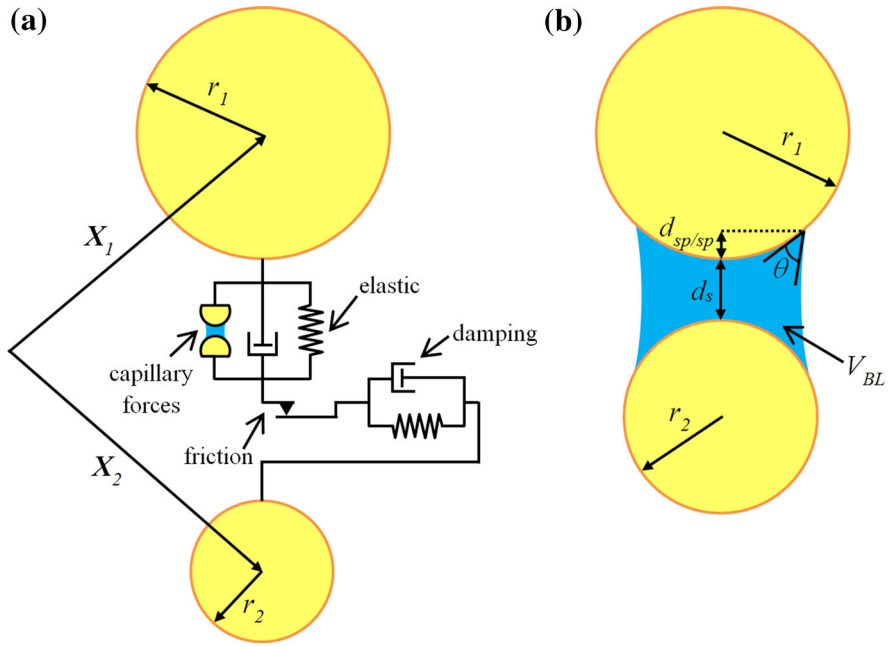

Fig. 3 **a** Particle–particle contact interaction; **b** Schematic of a liquid bridge between two particles

$$F_{fr} = fricF_N \tag{9}$$

where *fric* is the coefficient of friction and F_N is the sum of the normal forces F_n and F_{ndamp}. Rolling resistance of a particle is introduced via a moment M_r that tends to delay rolling motion (Karajan et al. 2014),

$$M_r = fricrF_N \tag{10}$$

where *fricr* is a user-defined rolling friction parameter.

An important factor in DEM modelling is the correct determination of material input parameters at the micro-scale or particle level, e.g. contact properties and cohesion between particles, which can produce bulk response predictions (Coetzee and Nel 2014). Determination of these microparameters is challenging because it is not always possible to measure them directly through experiment (Coetzee and Nel 2014). However, calibration methods have been developed, in which, numerical tests are employed to calibrate parameters individually through an iteration process until an experimentally observed bulk response is predicted (Grima and Wypych 2011; Jensen et al. 2014; Karajan et al. 2014a, 2015; Coetzee and Nel 2014; Coetzee and Els 2009; Gröger and Katterfeld 2006).

3.2 Capillary force model

Capillary forces between wet particles are taken into account via the capillary bridge model developed by Rabinovich et al. (2005), which is implemented in the recent version of LS-DYNA (version R8.0). In this model, a liquid bridge with fixed volume V_{LB} between two spheres with radii r_1 and r_2, respectively, and separated by a distance d_s (Fig. 3b), produces a capillary force given by (Hallquist 2015),

$$F_{sp/sp} = -\frac{2\pi R\gamma\cos(\theta)}{1+\frac{d_s}{2d_{sp/sp}}} \tag{11}$$

where γ is the liquid surface tension, θ is the contact angle, $R = 2r_1r_2/(r_1+r_2)$ is the effective radius and $d_{sp/sp}$ is the immersion distance given by,

$$d_{sp/sp} = \frac{d_s}{2}\left(-1+\sqrt{1+\frac{2V_{LB}}{\pi Rd_s^2}}\right) \tag{12}$$

The liquid bridge exists when d_s is less than or equal to the rupture distance $d_{crit} = \left(1+\frac{\theta}{2}\right)\sqrt[3]{V_{LB}}$ (Lian et al. 1993). The liquid bridge volume is defined by (Karajan et al. 2015),

$$V_{LB} = \frac{4}{3}\pi\left(r_1^3+r_2^3\right)\frac{1}{10}VOL \tag{13}$$

where *VOL* is a user-defined volume fraction of the liquid bridge between two particles to take into account how wet the particles are, depending on the water saturation ($0 < VOL \leq 1$). In LS-DYNA, saturation cannot be used directly as an input and therefore *VOL* has to be estimated. A simple way to estimate the parameter *VOL*, assuming uniform particles and uniform water distribution between them, is by knowing V_{LB} from the water saturation and assuming $r_1 = r_2 = \bar{r}$ in Eq. (13), where $\bar{r}$ is the average particle radius. V_{LB} can be estimated as $V_{LB} = V_W/N_{LB}$, where V_W is the volume of water and N_{LB} is number of liquid bridges. V_W can be calculated as,

$$V_W = S\varphi V \tag{14}$$

where S is the water saturation, φ is the porosity and V is the total volume of the specimen. N_{LB} can be estimated as,

$$N_{LB} = \frac{n_c}{2}N_p \tag{15}$$

where n_c is the average coordination number of a single particle defined as the total number of contact points with surrounding particles (Rietema 1991) and N_p is the number of particles. The $\frac{1}{2}$ factor in Eq. (15) stems from the fact that two particles shared a contact point. As an example of using the aforementioned procedure, for the drop test specimen described in Sect. 2.3 with $S = 10$ %, $VOL = 0.16$ was used for the simulations in Sect. 4.2. The materials properties shown in Table 1 were used to model DEM sand particles. The surface tension of water used in the simulations was $\gamma = 0.072$ N/m.

4 Results and discussion

4.1 Slump test on a horizontal surface

Figure 4a shows typical shapes of the sand pile after test. From these photographs, the height H of the pile and the angle of repose α were quantified (Table 2). These results were also used to calibrate the values of the DEM contact parameters rolling friction *fricr* and

Table 1 Material properties

Material properties	Sand	Steel plate and bars	Polyolefin
Density ρ (kg/m^3)	2650	7800	1200
Elastic modulus E (GPa)	70	210	0.01
Poisson's ratio	0.2	0.3	0.37

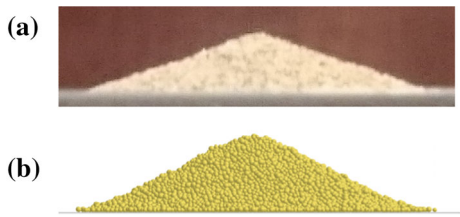

Fig. 4 Comparison of the angle of repose and height from slump test of dry sand for **a** experiment, and **b** simulation

dynamic friction *fricd*, which are shown in Table 3. Damping parameters (*ndamp* and *tdamp*) were fixed to 0.7 (Karajan et al. 2014) and contact friction *fric* and static friction *frics* were taken from the literature (Table 3). The sizes of the particles used in DEM simulations to approximate sand grain sizes are shown in Table 4. It can be seen that with these parameters values, the shape of the pile of sand from DEM simulation (Fig. 4b) agrees very well with the experiment. This is further confirmed by the numerically-obtained values of H and α, which are 7.2 mm and 23.1°, respectively.

4.2 Drop test

Figure 5 shows photographs of sand piles after drop test for various drop heights h and saturations S. It can be seen that for $h = 25$ cm, the piles at the centre are higher and tend to have a more regular pyramidal shape when compared to $h = 75$ cm. For $h = 75$ cm, the piles have a more irregular shape due to higher kinetic energy at impact point. It can be seen in Table 2 and Fig. 6 that the higher the saturation degree, the higher the sand pile. This might be due to higher cohesion between particles for larger saturation levels within the tested saturation range (10–30 %).

Figure 7 shows splash patterns of partially saturated sand after impact. The area shown in each image is 120 mm × 120 mm. For a drop height of 25 cm, it can be seen that for lower saturation degree, the sand ejecta are further away from the impact centre when compared to larger saturation. Also, the ejecta sizes are smaller for lower saturation degrees. For a drop height of 75 cm, it is not clear from Fig. 7 whether the ejecta are larger or travel further from the impact centre for lower saturation degree when compared to higher saturation degree. This may be due to the fact that the larger kinetic energy for this drop height does

Table 3 DEM parameters in LS-DYNA

DEM parameters	
NDAMP	0.7 (Karajan et al. 2014)
TDAMP	0.7 (Karajan et al. 2014)
fric	0.6 (Uesugi and Kishida 1986)
fricr	0.1
frics	0.3 (Karajan et al. 2012)
fricd	0.3

Table 2 Experimental and numerical results

Test			Height H (mm)		Angle of repose α (°)	
			Experiment	Simulation	Experiment	Simulation
Slump test			7.0	7.2	21.3 ± 0.9	23.1
Drop test	$h = 25$ cm	$S = 10$ %	6.8 ± 0.4	5.4	–	–
		$S = 20$ %	7.4 ± 0.4	5.5	–	–
		$S = 30$ %	8.3 ± 0.5	5.7	–	–
	$h = 75$ cm	$S = 10$ %	4.6 ± 0.6	4.5	–	–
		$S = 20$ %	5.0 ± 0.1	4.6	–	–
		$S = 30$ %	6.2 ± 0.2	5.5	–	–

Table 4 Particle sizes used in DEM specimens

Material	Sizes (percentages)
Poorly graded river sand	0.26 (36 %), 0.36 (49 %), 0.46 (15 %)
Quikrete #1961 sand (Kabir et al. 2010)	0.24 (7 %), 0.3 (14 %), 0.4 (22 %), 0.5 (15 %), 0.6 (27 %), 0.8 (15 %)

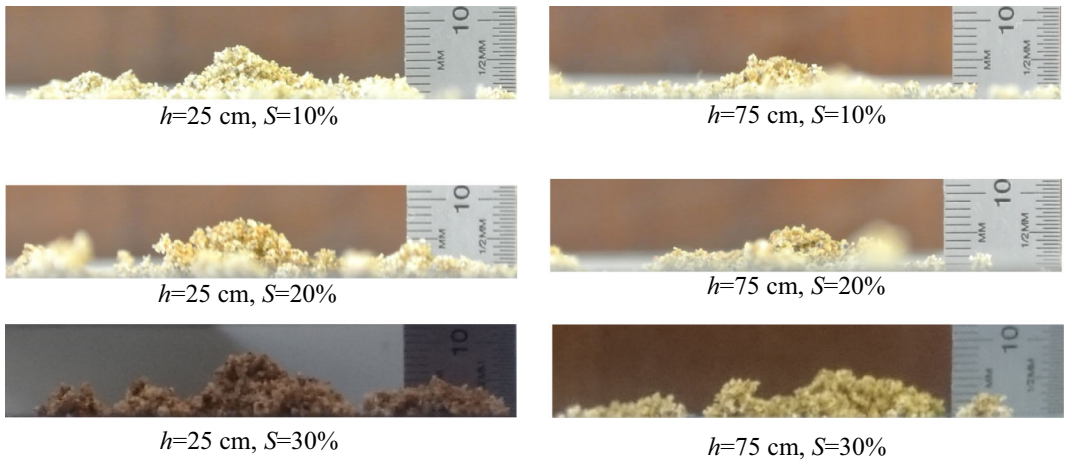

Fig. 5 Comparison of sand pile after impact for drop heights and saturation degrees

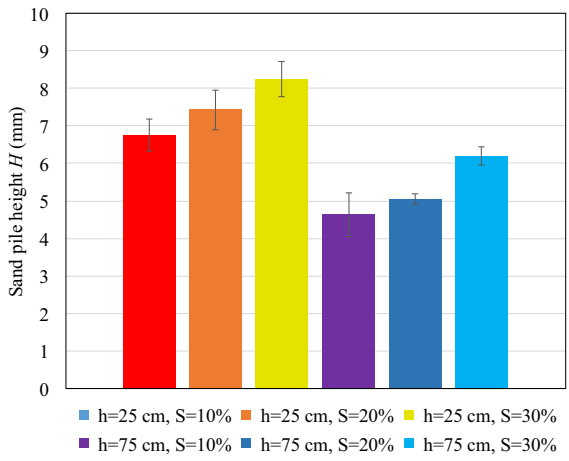

Fig. 6 Comparison of sand pile height H after impact for drop heights and saturation degrees

not produce a visible difference in this range of saturation. Further experimental and numerical tests will therefore be needed in the future to explore and quantify the competing effects of saturation and height on the ejecta.

Figures 8 and 9 show the numerical results for drop heights of 25 and 75 cm, respectively, for various capillary force parameters. It can be seen that the patterns are captured well for $H = 25$ cm for 10 and 20 % saturation when a contact angle θ of 40° is used; however, for contact angles larger than 40° the sand ejecta travel further away from the impact centre. The height of the sand pile predicted numerically (Tables 2, 5) at the impact centre is underestimated by about 20 % when compared to the experimental results in Table 2. This may be due to the fact that the simulated DEM particles are spherical, thus resulting in less contact points as compared to irregular sand particles in experiments.

4.3 Split Hopkinson pressure bar test

To further investigate the effect of capillary forces on the dynamic response of sand at high strain rate loading conditions, a DEM–FEM simulation of the SHPB test was performed with the same setup as that presented by (Kabir et al. 2010; Song et al. 2009). In this setup, a dry sand (Quikrete #1961 sand) specimen 19 mm in diameter and 9.3 mm in length was placed between steel bars with 19-mm diameter. A polyolefin heat shrink tube was used to keep the specimen in place while providing a low level of confinement

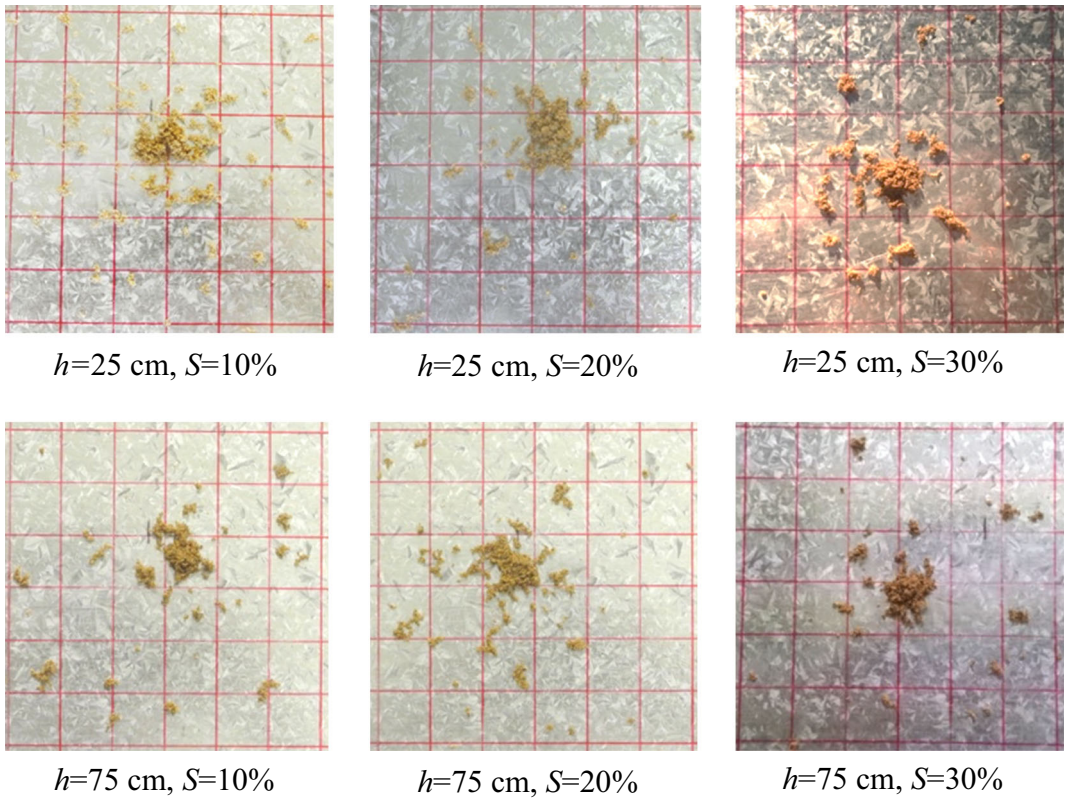

Fig. 7 Top view of of splash patterns of sand specimen after impact for different drop heights and saturation degrees

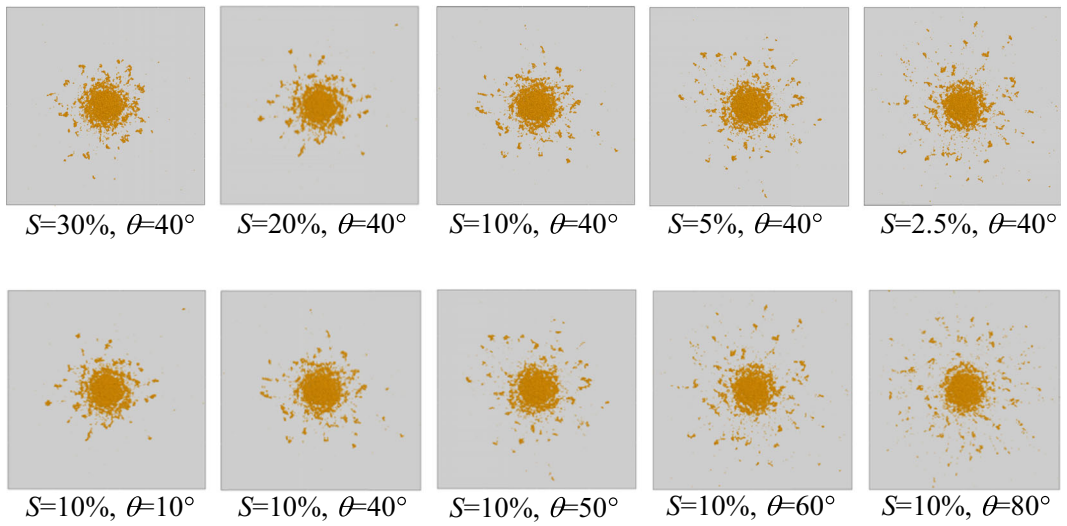

Fig. 8 Top view of sand particles after numerical simulations of drop test at $h = 25$ cm for different capillary forces parameters

(Song et al. 2009). Low level of confinement was chosen for our simulations in order to minimise grain crushing since DEM particles implemented in LS-DYNA R8.0 cannot capture this behaviour. The input and output bars of the SHPB and the polyolefin tube were modelled with FEM (8-node brick elements with

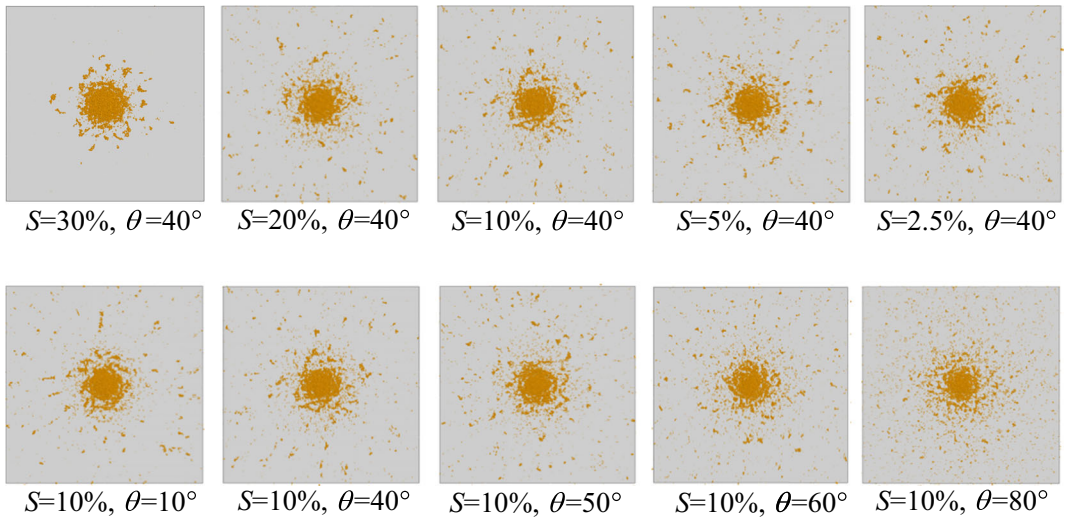

Fig. 9 Top view of sand particles after numerical simulations of drop test at $h = 75$ cm for different capillary forces parameters

Table 5 Numerical results for drop test

Test	Height H (mm) Simulation
$h = 25$ cm	
$S = 2.5$ %, $\theta = 40°$	5.2
$S = 5.0$ %, $\theta = 40°$	5.4
$S = 10$ %, $\theta = 40°$	5.4
$S = 20$ %, $\theta = 40°$	5.5
$S = 30$ %, $\theta = 40°$	5.7
$S = 10$ %, $\theta = 80°$	4.0
$S = 10$ %, $\theta = 60°$	5.1
$S = 10$ %, $\theta = 50°$	5.2
$S = 10$ %, $\theta = 40°$	5.4
$S = 10$ %, $\theta = 10°$	5.7
$h = 75$ cm	
$S = 2.5$ %, $\theta = 40°$	4.3
$S = 5.0$ %, $\theta = 40°$	4.5
$S = 10$ %, $\theta = 40°$	4.5
$S = 20$ %, $\theta = 40°$	4.6
$S = 30$ %, $\theta = 40°$	5.2
$S = 10$ %, $\theta = 80°$	3.1
$S = 10$ %, $\theta = 60°$	4.2
$S = 10$ %, $\theta = 50°$	4.4
$S = 10$ %, $\theta = 40°$	4.5
$S = 10$ %, $\theta = 10°$	4.7

reduced integration) using an isotropic elastic material with properties summarized in Table 1. DEM parameters shown in Table 3 were used for SHPB simulations. The specimen was modelled using DEM particles with diameters listed in Table 4 (Quikrete #1961 sand) (Kabir et al. 2010). The total number of particles are 19,770 for the specimen and the total number of FEM elements are 13,447 for each pressure bar and 46,080 for the tube. Contact between particles and FEM elements was defined using the AUTOMATIC_NODES_TO_SURFACE contact option. An incident wave similar to that shown in (Kabir et al. 2010) was applied to the impact end of the incident bar as a stress pulse. The trapezoidal incident wave has rising time, loading time and unloading time of 100, 300 and 100 μs, respectively, with a peak stress of 100 MPa.

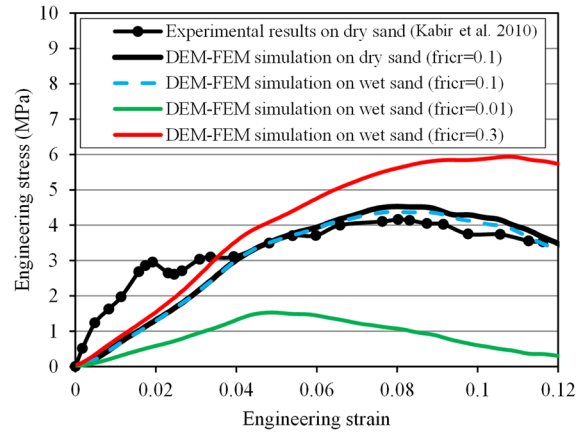

Fig. 10 Comparison of experimental results from (Kabir et al. 2010) and DEM simulations

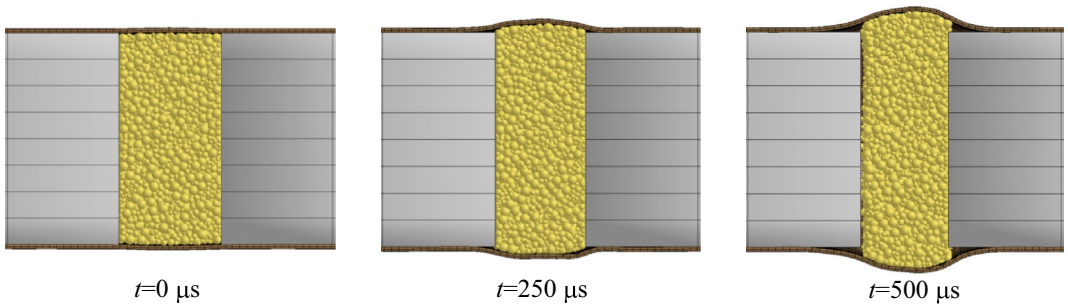

Fig. 11 DEM–FEM simulation of the deformation process of dry sand specimen in SHPB test

Figure 10 shows a comparison of stress–strain curves from experiments in (Kabir et al. 2010) for dry sand with results from DEM–FEM simulations for both dry and wet sand. Simulations matched the experimental curves well at the peak strength and unloading part; however, the initial stiffness was not captured by the simulations. An increase in rolling friction ($fricr = 0.3$ in Fig. 10) led to a slight increase of the stiffness; however, this increase was not sufficient to match the stiffness observed experimentally possibly because DEM particles were spherical and led to less contacts points when compared to irregular sand particles. Karajan et al. (Karajan et al. 2014) explained that rolling friction in LS-DYNA is a workaround for non-spherical systems and might not be sufficient to mimic the behaviour of irregular shaped grains in dynamic conditions. Despite the low level of confinement, which allowed particles to move sideways from the loading direction (Fig. 11), grain crushing may have occurred in the SHPB testing, which could not be captured with traditional DEM particles.

In addition, a case with 20 % saturation was modelled and is presented in Fig. 10. It can be seen that the DEM simulation curve for wet sand was very close to the dry sand curve. This indicated that for this particular setup, capillary forces did not play an important role in the stress–strain response. Moreover, a case with very low rolling friction ($fricr = 0.01$) showed a reduction in stiffness and peak strength. This observation is very interesting because it indicates that if water content reduces friction between particles as suggested by Martin et al. (Martin et al. 2009), this may explain the reduction of stiffness observed experimentally for saturations in the range of 3–20 % when compared to dry sand (Martin et al. 2009). It is noted that effects of the assumption of homogeneity in water distribution for capillary forces (Eqs. 13–15) and dynamic effects of fluid viscosity on the results were not assessed. We acknowledge that further simulations have to be performed to support these numerical observations, particularly simulations that can explicitly capture grain crushing and water-grain interactions.

5 Conclusions

An experimental and numerical investigation of the behaviour of partially saturated sand subjected to dynamic loading was presented in this study. We aimed to explore the capability of the DEM and the implicit capillary contact model in LS-DYNA for modelling the dynamic behaviour of partially saturated sand under impact loading. Slump tests were performed on dry sand to calibrate contact parameters in DEM simulations. Low-velocity-impact drop tests were performed to validate the simulations and investigate the effect of capillary forces on the shape and height of sand piles after impact. It was found that the higher the water saturation, the higher the sand pile becomes for a given drop height due to larger suction induced cohesion between particles [within the tested saturation range (10–30 %)]. The simulations captured well the main physical observations in the experiment such as ejecta patterns and reduction of pile sand height with the increase of drop height; however, the ejecta were smaller than those in the experiments for the higher drop heights.

In addition, SHPB with low confinement test was modelled and the simulation results were compared with available experimental data. It was found that the simulations can capture general trends of the stress–strain curve such as maximum stress and unloading.

The predicted stiffness was smaller than the reported experimental stiffness. This may be due to the fact that grain crushing cannot be captured with current DEM implementation and water is modelled implicitly.

As concluding remarks, our DEM–FEM simulations show that it is feasible to model dynamic behaviour of wet sand in LS-DYNA including high strain rate behaviour with low confinement; however, careful calibration of numerical parameters is recommended. For more complex cases with grain crushing and/or large saturation, it is expected that the simulations can capture only general trends unless complex crushing mechanisms at the grain scale and irregular grain shape are properly taken into account, and pore water is modelled explicitly. This is a direction for our on-going research.

Acknowledgments This work was supported in part by the Australian Research Council Discovery Projects (DP140100945), and the National Natural Science Foundation of China (No. 11232003). This research was undertaken with the assistance of resources from the National Computational Infrastructure (NCI), which is supported by the Australian Government.

References

Shahbodagh-Khan, B., Khalili, N., Alipour Esgandani, G.: A numerical model for nonlinear large deformation dynamic analysis of unsaturated porous media including hydraulic hysteresis. Comput. Geomech. **69**, 411–423 (2015)

Omidvar, M., Iskander, M., Bless, S.: Stress–strain behavior of sand at high strain rates. Int. J. Impact Eng **49**, 192–213 (2012)

Martin, B.E., Chen, W., Song, B., Akers, S.A.: Moisture effects on the high strain-rate behavior of sand. Int. J. Impact Eng **41**, 786–798 (2009)

Saleh, M., Edwards, L.: Evaluation of soil and fluid structure interaction in blast modelling of the flying plate test. Comput. Struct. **151**, 96–114 (2015)

Mitarai, N., Nori, F.: Wet granular materials. Adv. Phys. **55**, 1–45 (2006)

Veyera, G.E.: Uniaxial Stress–Strain Behavior of Unsaturated Soils at High Strain Rates. Wright Laboratory, Flight Dynamics Directorate, Tyndall AFB (1994)

Horn, H.M., Deere, D.U.: Frictional Characteristics of Minerals. Géotechnique **12**, 319–335 (1962)

Takita, H., Sumita, I.: Low-velocity impact cratering experiments in a wet sand target. Phys. Rev. E **88**, 022203 (2013)

Park, S., Uth, T., Fleck, N.A., Wadley, H.N.G., Deshpande, V.S.: Sand column impact onto a Kolsky pressure bar. Int. J. Impact Eng **62**, 229–242 (2013)

Kong, X., Fang, Q., Hong, J., Wu, H.: Numerical study of the wake separation and reattachment effect on the trajectory of a hard projectile. Int. J. Prot. Struct. **5**, 97–118 (2014)

Li, Q.M., Flores-Johnson, E.A.: Hard projectile penetration and trajectory stability. Int. J. Impact Eng **38**, 815–823 (2011)

Omidvar, M., Iskander, M., Bless, S.: Response of granular media to rapid penetration. Int. J. Impact Eng **66**, 60–82 (2014)

Børvik, T., Olovsson, L., Hanssen, A.G., Dharmasena, K.P., Hansson, H., Wadley, H.N.G.: A discrete particle approach to simulate the combined effect of blast and sand impact loading of steel plates. J. Mech. Phys. Solids **59**, 940–958 (2011)

Borg, J.P., Morrissey, M.P., Perich, C.A., Vogler, T.J., Chhabildas, L.C.: In situ velocity and stress characterization of a projectile penetrating a sand target: experimental measurements and continuum simulations. Int. J. Impact Eng **51**, 23–35 (2013)

Alonso-Marroquín, F., Herrmann, H.J.: The incremental response of soils: an investigation using a discrete-element model. J. Eng. Math. **52**, 11–34 (2005)

Alonso-Marroquín, F., Wang, Y.: An efficient algorithm for granular dynamics simulations with complex-shaped objects. Granul. Matter **11**, 317–329 (2009)

Gan, Y., Kamlah, M.: Discrete element modelling of pebble beds: with application to uniaxial compression tests of ceramic breeder pebble beds. J. Mech. Phys. Solids **58**, 129–144 (2010)

Alonso-Marroquín, F., Ramírez-Gómez, Á., González-Montellano, C., Balaam, N., Hanaor, D.H., Flores-Johnson, E.A., Gan, Y., Chen, S., Shen, L.: Experimental and numerical determination of mechanical properties of polygonal wood particles and their flow analysis in silos. Granul. Matter **15**, 811–826 (2013)

Dwivedi, S.K., Teeter, R.D., Felice, C.W., Gupta, Y.M.: Two dimensional mesoscale simulations of projectile instability during penetration in dry sand. J. Appl. Phys. **104**, 083502 (2008)

Oñate, E., Rojek, J.: Combination of discrete element and finite element methods for dynamic analysis of geomechanics problems. Comput. Methods Appl. Mech. Eng. **193**, 3087–3128 (2004)

Scholtès, L., Chareyre, B., Nicot, F., Darve, F.: Discrete modelling of capillary mechanisms in multi-phase granular media. CMES Comput. Model. Eng. Sci. **52**, 297–318 (2009)

Grima, A., Wypych, P.: Development and validation of calibration methods for discrete element modelling. Granul. Matter **13**, 127–132 (2011)

Gröger, T., Tüzün, U., Heyes, D.M.: Modelling and measuring of cohesion in wet granular materials. Powder Technol. **133**, 203–215 (2003)

Gan, Y., Maggi, F., Buscarnera, G., Einav, I.: A particle-water based model for water retention hysteresis. Geotech. Lett. **3**, 152–161 (2013)

Elperin, T., Golshtein, E.: Comparison of different models for tangential forces using the particle dynamics method. Phys. A **242**, 332–340 (1997)

Flores-Johnson, E.A., Li, Q.M.: Low velocity impact on polymeric foams. J. Cell. Plast. **47**, 45–63 (2011)

Cundall, P.A., Strack, O.D.L.: A discrete numerical model for granular assemblies. Géotechnique **29**, 47–65 (1979)

Hallquist, J.O.: LS-DYNA Keyword User's Manual, Version R8.0. Livermore Software Technology Corporation, California (2015)

Jensen, A., Fraser, K., Laird, G.: Improving the precision of discrete element simulations through calibration models.

In: 13th International LS-DYNA Conference, Detroit (2014)

Pandey, P., Song, Y., Turton, R.: Chapter 8 modelling of pan-coating processes for pharmaceutical dosage forms. In: Salman, M.J.H.A.D., Seville, J.P.K. (eds.) Handbook of Powder Technology, pp. 377–416. Elsevier Science B.V, Amsterdam (2007)

Wriggers, P.: Computational Contact Mechanics, 2nd edn. Berlin, Springer (2006)

Karajan, N., Han, Z., Teng, H., Wang, J.: On the parameter estimation for the discrete-element method in LS-DYNA. In: 13th International LS-DYNA Conference, Detroit (2014)

Karajan, N., Lisner, E., Han, Z., Teng, H., Wang, J.: Particles as discrete elements in LS-DYNA: interaction with themselves as well as deformable or rigid structures. In: 11th LS-DYNA Forum, Ulm (2012)

Karajan, N., Asperberg, D., Teng, H., Han, Z., Wang, J.: Workshop on the discrete-element method in LS-DYNA. In: 10th European LS-DYNA Conference, Würzburg (2015)

Coetzee, C.J., Nel, R.G.: Calibration of discrete element properties and the modelling of packed rock beds. Powder Technol. **264**, 332–342 (2014)

Coetzee, C.J., Els, D.N.J.: Calibration of discrete element parameters and the modelling of silo discharge and bucket filling. Comput. Electron. Agric. **65**, 198–212 (2009)

Grger, T., Katterfeld, A.: On the numerical calibration of discrete element models for the simulation of bulk solids. In: Marquardt, W., Pantelides, C. (eds.) Computer Aided Chemical Engineering, pp. 533–538. Elsevier, Amsterdam (2006)

Rabinovich, Y.I., Esayanur, M.S., Moudgil, B.M.: Capillary forces between two spheres with a fixed volume liquid bridge: theory and experiment. Langmuir **21**, 10992–10997 (2005)

Lian, G., Thornton, C., Adams, M.J.: A theoretical study of the liquid bridge forces between two rigid spherical bodies. J. Colloid Interface Sci. **161**, 138–147 (1993)

Rietema, K.: The Dynamics of Fine Powders. Elsevier, Amsterdam (1991)

Uesugi, M., Kishida, H.: Influential factors of friction between steel and dry sands. Soils Found. **26**, 33–46 (1986)

Kabir, M.E., Song, B., Martin, B.E., Chen, W.: Compressive behavior of fine sand. Sandia National Laboratories, New Mexico (2010)

Song, B., Chen, W., Luk, V.: Impact compressive response of dry sand. Mech. Mater. **41**, 777–785 (2009)